OLHA (N^{α}-oleoylhistamine) modulates activity of mouse brain histaminergic neurons

Olga A. Sergeeva[1,2*], Karolina Mazur[2], David Reiner-Link[3], Kiril Lutsenko[3], Helmut L. Haas[1], Mercedes Alfonso-Prieto[4,5#] and Holger Stark[3#]

[1] Institute of Neural and Sensory Physiology, Medical Faculty, Heinrich Heine University Düsseldorf, 40225 Düsseldorf, Germany

[2] Institute of Clinical Neurosciences and Medical Psychology, Medical Faculty, Heinrich Heine University Düsseldorf, 40225 Düsseldorf, Germany

[3] Institute of Pharmaceutical and Medicinal Chemistry, Heinrich Heine University Düsseldorf, 40225 Düsseldorf, Germany

4 Cécile and Oskar Vogt Institute for Brain Research, Medical Faculty, Heinrich Heine University Düsseldorf, 40225 Düsseldorf, Germany

5 Computational Biomedicine, Institute for Advanced Simulation IAS-5/Institute for Neuroscience and Medicine INM-9, Forschungszentrum Jülich GmbH, 52425 Jülich, Germany

# equal contribution to the study

Running Title: OLHA action in the hypothalamus

Declaration of interests: none

* Corresponding Author:

Olga A. Sergeeva
Institute of Neural and Sensory Physiology
Institute of Clinical Neurosciences and Medical Psychology
Heinrich-Heine-University, Medical Faculty,
D – 40225 Düsseldorf
Germany
Tel 0049 211 8112696
e-mail: olga.sergeeva@uni-duesseldorf.de

Abstract

Histaminergic (HA) neurons are located in the tuberomamillary nucleus (TMN) of the posterior hypothalamus, from where they project throughout the whole brain to control wakefulness. We examined the effects of N^{α}-oleoylhistamine (OLHA), a non-enzymatic condensation product of oleic acid (OLA) and histamine, on activity of mouse HA neurons in brain slices. OLHA bidirectionally modulated the firing of HA neurons. At 10nM OLHA inhibited or had no action, whereas at 1µM it evoked excitatory and inhibitory responses. Inhibition was not seen in presence of the histamine receptor H3 (H_3R) antagonist clobenpropit and in calcium-free medium. Pre-incubation with a histamine-reuptake blocker prevented the decrease in firing by OLHA. OLHA-evoked increase in firing (EC_{50} ~44nM) was insensitive to blockers of cannabinoid 1 and 2 receptors and of the capsaicin receptor, but was significantly impaired by the peroxisome proliferator-activated receptor-alpha (PPAR-alpha) antagonist MK886, which suppressed also the rise in intracellular calcium level caused by OLHA. The OLHA-evoked excitation was mimicked by synthetic PPAR-alpha agonists (gemfibrozil and GW7647) and was abolished by the PKA inhibitor H-89. The H_3R affinity (Ki) for histamine, measured in HEK293 cells with stable expression of human H_3R, was higher than for OLHA (Ki: 42 vs 310nM, respectively). Expression of PPAR-alpha was not different between TMN regions of males and females, responses to OLHA did not differ. Molecular modelling of PPAR-alpha bound to either OLHA or OEA showed similar binding energies. These findings shed light on a novel biotransformation product of histamine which may play a role in health and disease.

Keywords: Histamine receptor H3; PPAR-alpha; patch-clamp; posterior hypothalamus; HEK293; in silico electrophysiology

Highlights

OLHA bidirectionally modulates histaminergic neuron firing.

Histamine 3 receptor and PPAR-alpha are involved in inhibition and excitation respectively.

OLHA interacts with histamine reuptake and may modulate histaminergic transmission under pathological conditions

1. Introduction

Brain histaminergic neurons, located solely in the tuberomamillary nucleus (TMN) of posterior hypothalamus, fire at highest rate during wakefulness controlling cortical arousal and are silent during slow wave sleep (Haas, Sergeeva, and Selbach 2008; Panula et al. 2015); in addition, they regulate feeding and stimulate energy expenditure (Yasuda et al. 2004; Provensi et al. 2014) through mechanisms not completely understood. There are 4 known metabotropic histamine receptors in mammals (Panula et al. 2015); however, some effects of histamine are not mediated through these receptors. The condensation products of oleic acid (OLA) with catecholamines (like OLDA, a conjugate of OLA and dopamine) possess neuromodulatory activities (Sergeeva et al. 2017; De Luca et al. 2018), including block of transmitter reuptake and interaction with cannabinoid- and vanilloid- receptors. Interestingly, a similar condensation product between OLA and histamine (OLHA) exists, which induces expression of PPAR-alpha target genes in liver cell lines with an efficacy similar to oleoylethanolamide (OEA) (Takao et al. 2015). Nothing is known about neural activity of OLHA. Synthetic PPAR-alpha ligands, such as gemfibrozil, are in clinical use to treat hyperlipidemia (Rubins et al. 1999; Frick et al. 1987). Production of endogenous PPAR-alpha activators may be increased under the conditions when OLA concentration is high, such as starvation (Kamata et al. 2020) or neurodegeneration (Fanning et al. 2019); they may serve neuroprotection as some synthetic PPAR-alpha activators do (Agarwal, Yadav, and Chaturvedi 2017; Avagliano et al. 2016; Gottschalk et al. 2019; Plaza-Zabala et al. 2010). The potencies of OLHA at PPAR-alpha and possibly other targets were not determined in native systems so far. Here we test the action of a highly purified condensate between OLA and histamine (N^{alpha}-oleoylhistamine, OLHA) on electrophysiological activity and intracellular calcium^{2+} levels of mouse histaminergic (HA) neurons in the TMN which control cortical arousal (Haas et al., 2008;Panula et al., 2015). These neurons express only one type of histamine receptors, namely the H_3R (histamine H_3 receptor) (De Luca et al. 2016). OLHA at 10nM inhibited the firing of HA neurons most likely by blocking the histamine-reuptake system with subsequent increase in extracellular histamine level and H_3R activation. In HEK293 cells stably expressing hH_3R, OLHA at 10nM was inactive, whereas starting from 30nM it competed with [^{3}H]- N^{α}-methylhistamine binding. At higher concentrations (100nM, 1µM) OLHA evoked in mouse HA cells both, excitatory and inhibitory effects. A detailed pharmacological analysis of these responses is provided. Molecular modelling showed that

the binding energy of OLHA to PPAR-alpha is similar to that of OEA and only slightly lower than that of the most potent PPARalpha synthetic agonist, GW7647.

2. Methods

2.1 Animals

In electrophysiological experiments juvenile and adult mice of both sexes were used; expression of the fluorescent Tomato protein under control of the histidine decarboxylase promoter Tmt-HDC helped to visualize living histaminergic neurons (Yanovsky et al. 2012). Both parent lines: HDC-Cre (generous donation from Prof. Jeffrey Zigman at UT Southwestern Medical Center) and B6J/N. Cg-Gt(ROSA)26Sortm14(CAG−tdTomato) (from Jackson Laboratory #007908)- were bred separately and crossings between them were ordered only for the purpose to obtain experimental animals; all of them were used even though some mice did not carry both transgenes and will be further called “wild type”(WT). For GCaMP6f imaging the HDC-Cre parent line was crossed to the B6J.Cg-Gt(ROSA)26Sor$^{tm95.1(CAG-GCaMP6f)Hze}$/MwarJ (Stock No 028865, Jackson Laboratories, USA) to yield expression of the calcium indicator exclusively in histaminergic neurons of TMN. All mice had a C57Bl6 genetic background. This is the species generally used for neurobiology and in pharmacological research on PPAR-alpha (Dotson et al. 2016) and H_3R (De Luca et al. 2016). The human histamine receptor H3 (H_3R) displays a different potency of antagonists but the same potency of agonists compared to the mouse H_3R (Yao et al. 2003). Animals were held at 12/12 hrs. dark/light cycle, temperature 18-22 °C, 55% humidity and free access to water and food under specific pathogen-free conditions. Mice were housed 2 to 5 per cage. All procedures were in compliance with the guidelines for the use of experimental animals, as given by the Directive 2010/63/EU of the European Parliament, the German “Tierschutzgesetz” (animal protection law) and approved by the local authorities (LANUV NRW: Landesamt für Umwelt, Natur und Verbraucherschutz Nordrhein Westfalen, Bezirksregierung Düsseldorf; permission number O58/91). Before decapitation two weeks of age or older mice were anaesthetized with isoflurane. All efforts were made to minimize number of animals and their suffering.

2.2 Slice preparation and electrophysiology

From postnatal day 9 to nine month old mice were used for electrophysiological *ex-vivo* recordings. Patch-clamp data reported in this study were obtained from 126 mice (82 carried both: CAG−tdTomato (Tmt) and HDC-Cre transgenes, further called "Tmt-HDC"), among those 50 were not older than postnatal day 14 (P14) and will be further called "juvenile" (P11.56± 0.23) and 76 will be referred as "adult" (P55.6 ±5.8). Coronal brain slices from the posterior hypothalamus with a thickness of 250 µm containing the TMN were prepared using a tissue slicer (HR2, Sigmann Elektronik, Germany) in ice-cold artificial cerebrospinal fluid (ACSF) continuously bubbled with carbogen (5% CO_2/95% O_2) to maintain pH 7.4 (in mM): Sucrose 202, D-Glucose 12, $NaHCO_3$ 26, KCl 3.75, NaH_2PO_4 * H_2O 1.25, $MgSO_4$ * $7H_2O$ 1.3, $CaCl_2$ * $2H_2O$ 2. Further incubation steps and slice electrophysiology were done in ACSF with 125 mM NaCl instead of 202 mM sucrose. This solution was also used in the patch pipettes for the extracellular recordings.

All recordings were done at 25 °C. In slice recordings HA neurons were identified under an upright fluorescent microscope using infrared-differential interference contrast (IR-DIC) and Tmt-HDC neurons were identified by both, IR-DIC and fluorescence. We have reported previously that the vast majority of Tmt-expressing ventrolateral TMN (TMNv) neurons show histamine-immunoreactivity (Yanovsky et al., 2012) and thus can be reliably detected in *ex-vivo* preparations. Recordings were done with an EPC7 patch-clamp amplifier (Heka Elektronik, Lambrecht/Pfalz, Germany) and a Digidata 1200 interface board (Axon Instruments, USA). Electrical signals were filtered between 0.5 and 10kHz, sampled at 20kHz and analyzed with pClamp9 software (Axon Instruments, USA). The patch pipettes (resistance 4-5 MΩ) were made from 1.5mm (OD) borosilicate glass (Science Products GmbH, Hofheim, Germany) using a micropipette puller (P-87, Sutter Instruments C., Novato, CA, USA). The frequency of extracellular action potentials was determined online in bins of 60s duration. For the current clamp recordings electrodes contained (in mM): KCl 130, NaCl 10, $MgCl_2$ 2, $CaCl_2$ 0.25, glucose 5, HEPES 5, EGTA 10, MgATP 5, MgGTP 0.3, pH7.2 adjusted with KOH 1M. In current clamp experiments only cells showing membrane potentials more negative than -42mV and firing action potentials with overshoot were recorded. In some experiments the membrane potential was hyperpolarized to -70mV prior to recording in order to prevent depolarization block in response to OLHA 1µM application. Histaminergic neurons not carrying red fluorescence were selected for the recordings if they were located in the TMNv region, had a soma diameter larger than 15µm, fired spontaneously, were depolarized and/or

increased firing under the H_3R antagonist clobenpropit (20µM) (Sergeeva et al. 2020) or were hyperpolarized and/or decreased firing under RAMH. Data are presented as the frequency change (Hz) in relation to the 7 min baseline (control) period. Control firing frequency of HA neurons in normal ACSF was 0.78±0.05Hz (51 cells) and in calcium-free ACSF 1.65±0.11Hz (228 cells). In all experiments, where agonist and antagonist were co-applied for 7 min, the antagonist was pre-applied for additional 7 minutes; activity during this period was considered as baseline.

2.3 Ca^{2+} imaging from HDC-GCaMP6f mice

Imaging data were obtained from HDC-GCaMP6f mice aged 39 to 188 days (P116±18, n=11, 7 males, 4 females). Slices of 250µm thickness were prepared, incubated before recording and recorded in a similar perfusion chamber with the same speed of perfusion of NSOL at room temperature as in electrophysiological experiments (see above). Fluorescence of GCaMP6f was excited by a monochromator (Polychrome IV; TILL Photonics, Gräfelfing, Germany) at 470 nm wavelength (Kim et al. 2016). Image series were captured at 1 Hz with an exposure time of 15 ms by a cooled 12-bit IMAGO CCD camera and digitized by a computer running the TILLvisION Multi-Color Ratio Imaging System (TILL Photonics). Imaging protocols were programmed and executed with the software TILLvisION and images were symmetrically binned 4x (to 160 x 120 pixels) to increase the signal-to-noise ratio as previously described (Fleischer et al. 2017). Individual cells were defined as regions of interest and intensity changes in fluorescence were analyzed. Neurons were identified by their strong rise in intracellular calcium after kainate (5 µM) application at the end of a measurement series. For the analysis two data transformations were performed: first, the difference in fluorescence (F) with a 5 min baseline period (F0) was calculated (fluorescence change); and second: the percentage of the maximal kainate response was obtained for every data point (normalized fluorescence). Only regions of interest (ROI) where not more than 15% difference was observed between 1st and 5th minute of baseline were considered for the statistical analysis.

2.4 [^{3}H]-*N*$^{\alpha}$-Methylhistamine hH_3R displacement assay

The procedure was performed as described previously (Khanfar et al. 2018). To determine radioligand displacement, compounds were incubated with membrane preparations (20 µg/well) of HEK293 cells stably expressing the human H3 receptor (hH_3R, cell line was a kind

gift from Prof. J.-C. Schwartz, Bioproject) and [^{3}H]-N^{α}-methylhistamine (2 nM; K_D=3.08 nM as determined by saturation binding experiments) in a final assay volume of 200 µL. A buffer composed of 75 mM Tris, 100 mM NaCl, 10 mM $MgCl_2$; pH = 7.4) and ice-cold demineralized water were used as assay buffer and washing buffer for rapid filtration, respectively. Bound radioligand on filter mats was quantified by scintillation counting. Specific binding was analyzed by non-linear squares fit via GraphPad-Prism™ (2012, vers. 6.01, La Jolla, CA, USA). Affinities (K_i) were calculated from IC_{50}-values using the Cheng-Prusoff equation and expressed as means from at least five independent experiments in duplicates with 95% confidence intervals.

2.5 qRT-PCR detection of PPAR-alpha transcripts

As lower levels of PPAR-alpha expression were reported previously in ischemic brain of female mice compared to the male (Dotson et al., 2016) we quantified expression of PPAR-alpha in TMN regions prepared in the same way as for electrophysiological experiments with the real-time RT-PCR approach, further called “qRT-PCR”. TMN regions were dissected from 250µm-thick coronal slices from adult (postnatal day 60 (P60) to P103) or juvenile (P10-P13) mice and collected in the extraction buffer of mRNA isolation kit (GE Healthcare, GB). Protocols for mRNA purification and reverse transcription (RT) with the first strand cDNA synthesis kit (GE Healthcare, GB) are described elsewhere (De Luca et al. 2018). The qRT-PCR was performed using a StepOne Plus thermocycler and SybrGreen Master Mix reagents. Following the final cycle of the PCR, the reactions were heat denaturized over a 35 °C temperature gradient at 0.03 °C per second from 60 to 95 °C. Each PCR product considered for the analysis showed a single peak in the denaturation curve. All reactions were run in duplicates and normalized on the house-keeping gene Rpl13a (for primers see Sergeeva et al. 2020). Samples were diluted to contain about the same cDNA concentration (0.8+0.05 µg in 1µl, n=37). For the PPAR-alpha amplification the same primers as in De Luca et al (2018) were used (forward: 5´-ttc gga aac tgc ag acct-3` and reverse: 5´-aag cgt ctt ctg ggc cat ac-3´). Standard curves obtained from Rpl13a- and PPAR-alpha- amplifications of a serially diluted sample (as in (Sergeeva et al. 2003)) showed linear regression coefficients larger than 0.95. Therefore, we estimated mRNA levels of PPAR-alpha relative to Rpl13a (ΔCt) by the “$2^{-\Delta\Delta Ct}$“method, normalizing all reaction on ΔCt of calibrator (Sample #M10). Two or more amplifications were performed for each sample and averages (one per mouse) were

compared between 4 groups. Identity of PCR products with the known cDNA PPAR-alpha sequence for mouse (XM_030248424, Genbank NCBI) was confirmed by Sanger sequencing.

2.6. Molecular docking

The experimental results suggested that PPAR-alpha might mediate the excitatory effect of OLHA. In order to further investigate the possibility of OLHA binding at PPAR-alpha, molecular docking was used to generate *in silico* models of PPAR-alpha in complex with either OLHA or oleoylethanolamide (OEA). Comparison is also made with the crystal structures of PPAR-alpha bound to either oleic acid (OLA, PDB code 6LX8) or GW7647 (PDB code 6KB3) (Kamata et al. 2020), as well as to an *in silico* model of PPARalpha with gemfibrozil bound to the Center/Arm I region. All these ligands have been shown to bind to or activate PPAR-alpha (Kamata et al., 2020; Takao et al., 2015). To be the best of our knowledge, no molecular docking data have been published so far for OLHA.

The receptor structure (i.e. the human PPAR-alpha ligand binding domain, amino acids 202-468, see Supplementary Fig. 4) was taken from PDB code 6LX8 (Kamata et al., 2020) for the docking calculations of OEA and OLHA, and from PDB code 6KB3 for the docking of gemfibrozil. The two structures are almost identical, with a backbone RMSD of 0.86 Å. Residues unresolved in the X-ray structures were modeled with SwissModel (Waterhouse et al. 2018). The ligand structures of OEA and OLHA were built based on the OLA crystallographic pose in PDB 6LX8, by manually converting the carboxylate group into ethanolamine or histamine, respectively (see supplementary Fig. 4). Similarly, the initial ligand structure of gemfibrozil was obtained by manual superposition with the crystallographic pose of GW7647 in PDB 6KB3. Possible binding of gemfibrozil to a secondary site in the Arm II/X region of PPARalpha, as hypothesized in (Kamata et al. 2020), was not modeled here. Before docking, the ligand structures were optimized with the Molefacture plugin (version 2.0) of VMD (version 1.9.4a37) (Humphrey, Dalke, and Schulten 1996).

Docking was carried out using the Guru interface of the Haddock 2.2. webserver (van Zundert et al. 2016) using a template-based approach (Koukos, Xue, and Bonvin 2019). Hence, the receptor structures chosen (PDB codes 6LX8 and 6KB3) are the ones solved in complex with ligands similar to OEA and OLHA (OLA) and gemfibrozil (GW7647). The initial ligand structures

of OEA and OLHA are superimposed to the OLA crystallographic pose; this is also the case for gemfibrozil and GW7647. For each ligand, 200 docking poses were generated by flexible refinement of both receptor and ligand in the presence of explicit water.

To obtain statistics comparable with those of the docked complexes, the aforementioned crystallographic complexes of PPARalpha with OLA and GW7647 (PDB codes 6LX8 and 6KB3) (Kamata et al., 2020) were also submitted for refinement with the Haddock2.2. webserver. In the case of GW7647, the two conformers present in the X-ray structure were considered (hereafter denoted as A and B).

Binding affinities were calculated using the PRODIGY-LIG webserver (Xue et al. 2016). For the top 4 best scored poses, protein-ligand interactions were analyzed with the PLIP webserver (version 2.1.6) (Salentin et al. 2015). Default cutoff values were used: for hydrogen bonds, 4.1 Å maximum donor-acceptor distance and 100° minimum donor-hydrogen-acceptor angle; for hydrophobic interactions, 4.0 Å maximum carbon-carbon distance; for π stacking interactions, a 5.5 Å maximum distance between ring centers, 30° maximum deviation from the optimum stacking angle and 2.0 Å maximum offset between aromatic ring centers.

2.7 Statistical analysis

Data are presented as the mean ± SEM if not mentioned otherwise. Statistical analysis was performed using Excel and GraphPad Prism versions 5, 6.01 or 7.08 (La Jolla, CA, USA). We used the non-parametrical Mann Whitney U-test (MWT) for comparison between two groups, if no normal distribution of data was observed (statistical value reported as U(N1,N2), where N1: number of cells in group 1 and N2: number of cells in group 2), the unpaired t-test if data were normally distributed and had equal variances and the unpaired t-test with Welch´s correction for the comparison between two groups with normal distribution and unequal variances. One-way ANOVA, combined with appropriate posthoc tests, was used for the comparison of more than 2 groups if numbers within each group passed the Kolmogorov-Smirnov test for normal distribution. If no normal distribution was observed at least in one group, the Kruskal-Wallis test was used (reported as H(df,N)=statistical value, where df: degree of freedom (number of groups-1), N: total number of cells). For the comparison of response time-dependence between two drugs we used 2-way ANOVA with repeated measures (RM). The Wilcoxon signed rank test was used for comparison of baseline with the (post)application periods of the drug (Statistics W1.54, Oxford, UK). The difference in effect

probability was estimated with Fisher`s exact probability test (FEPT). A value of $p<0.05$ was considered statistically significant.

2.8 Drugs

Chemical compounds used in this study were the following (PubChem CID): AM251 (2125), AM630 (4302963) and clobenpropit (11213569) obtained from Tocris (Bio-Techne, Wiesbaden-Nordenstadt,Germany); AMG9810 (680502), Decynium 22 (D-22) (5484462), R-alpha-methylhistamine (156615), MK886 (4519262), kainate (10255), GW7647 (3392731), gemfibrozil (3463), H-89 dihydrochloride (5702541) were obtained from Sigma (Deisenhofen, Germany); tetrodotoxin (11174599) and gabazine (107896) obtained from Abcam (Cambridge, UK). Substances were diluted and stored as recommended by the provider. Working solutions were freshly prepared immediately before application. Concentration of DMSO in the ACSF did not exceed 0.1%.

We synthesized OLHA according to the previously published protocol (Takao et al. 2015). Synthesis, purification and analysis details are provided below.

Chemicals and materials: (*9Z*)-Octadec-9-enoic acid was purchased from Sigma Aldrich. Silica 60 (0.04-0.063 mm) for the column chromatography was purchased from Macherey Nagel. All other materials were obtained from regular suppliers.

Instrumentation: ^{1}H-NMR-was taken using Bruker Avance III-300 (300 MHz), ^{13}C-NMR-was taken using Bruker Avance III-300 (75 MHz). Liquid chromatography with coupled mass spectroscopy. Elute SP (HPG 700) Bruker Daltronics with vacuum-devolatilizer, autosampler, column oven, amaZon speed ETD (ESI-MS), Intensity Solo 2 C18 RP column 100 mm * 2.1 mm, 50 °C, Eluent: Acetonitrile (LC-MS-Grade, Sigma Aldrich, St. Louis, USA) and water (LC-MS-Grade, Sigma Aldrich, St. Louis, USA) with 0,1% formic acid.

Synthesis: (*9Z*)-Octadec-9-enoic acid (2.0 mmol) was dissolved in 20 mL CH_2Cl_2 and cooled in an ice bath. Thionyl chloride (10 mmol) in CH_2Cl_2 was added and the mixture was stirred at room temperature for 3 h. Solvent end excess of thionyl chloride were removed under reduced pressure and the corresponding acyl chloride was dissolved in *N,N*-dimethylformamide (DMF) (5 mL) and added dropwise to a suspension of histamine dihydrochloride (4.0 mmol) and Et_3N (16 mmol) in DMF (10 mL) cooled in an ice bath. The reaction mixture was stirred for 5 h at room temperature. Ice water was added to the mixture and it was extracted with CH_2Cl_2. The organic layer was dried over $MgSO_4$ anh. and

the solvent was evaporated under reduced pressure. The residue was purified by silica gel column chromatography (CH_2Cl_2: NH_3 sat. MeOH: =19: 1) to give N^{α}-oleoylhistamine (C18:1-Δ9-cis-HA: OLHA).

Analytics: Yield 86%; Colorless amorphous; mp 93–95°C; ^{1}H-NMR ($CDCl_3$, 300 MHz) δ: 8.37 (s, 1H), 7.57 (s, 1H), 6.81 (s, 1H), 6.63 (t, J = 5.7 Hz, 1H), 5.52 – 5.24 (m, 2H), 3.53 (q, J = 6.3 Hz, 2H), 2.82 (t, J = 6.6 Hz, 2H), 2.18 (t, J = 7.6 Hz, 2H), 2.06 – 1.95 (m, 4H), 1.61 (t, J = 7.5 Hz, 2H), 1.28 (d, J = 5.3 Hz, 20H), 0.97 – 0.79 (m, 3H); ^{13}C-NMR ($CDCl_3$, 75 MHz) δ: 173.75, 136.16, 134.92, 130.14, 129.86, 116.33, 39.42, 36.99, 32.02, 29.90, 29.85, 29.64, 29.45, 29.40, 29.29, 27.37, 27.33, 27.13, 25.90, 22.78, 14.18.; LC-MS 100% m/z 376,29 for $C23H42N3O^+$.

OLHA was made up as 10mM stocks in 100% DMSO, aliquots of which were stored at -20 °C.

3. Results

3.1 Dose dependence of OLHA action in histaminergic neurons

At a concentration of 10nM OLHA significantly reduced the firing frequency of 2 histaminergic neurons out of 7 in control and in 2 out of 8 in ACSF containing the $GABA_A$ receptor antagonist gabazine (10μM) with no difference in occurrence of inhibition (FEPT p=1.0; Supplementary Fig.1). OLHA at 1μM evoked often biphasic responses with a firing increase during the drug application period by 0.52±0.12Hz over baseline in 5 cells (in 5 other cells firing frequency was indistinguishable from the baseline, Wilcoxon signed rank test). During washout period (15th -21st min of experiment) either an inhibition of firing (to -1.6±0.57Hz from baseline, n=3 cells), excitation (3 cells, +0.9±0.57Hz) or no change (4 cells) occurred. Further experiments were performed with OLHA 1μM, as both components - inhibitory and excitatory - were clearly resolved at this concentration. Moreover, our previous studies on another conjugate of OLA and amine (dopamine), OLDA, in histaminergic and dopaminergic neurons were performed at 1μM (De Luca et al. 2018; Sergeeva et al. 2017).

3.2. Decrease of firing frequency by OLHA requires H_3R activation

We suspected involvement of H_3R in the inhibitory effect of OLHA, as OLDA (*N*-oleoyl-dopamine) inhibits dopaminergic neurons through D_2R by blocking dopamine uptake and increasing the extracellular level of dopamine (Sergeeva et al., 2017). In the presence of the H_3R antagonist clobenpropit (20μM) OLHA produced only excitation (+0.5±0.16Hz, n=7, 19th

-25th min of experiment), which was significantly different from baseline in 5 cells (Wilcoxon signed rank test, $p<0.05$) and not significant in 2 cells (Fig. 1A, Supplementary Fig.2). The difference in occurrence of excitation between control (n=10) and experiments in clobenpropit (n=7) was not significant (FEPT p=0.33). Two possibilities can explain the effects of OLHA: i) direct interaction with H_3R; ii) indirect, through inhibition of histamine uptake by the plasma membrane amino acid transporter (PMAT) or/and OCT3 (Courousse and Gautron 2015;Yoshikawa et al. 2013), which can lead to an increase of the extracellular histamine level and inhibition of firing through H_3R. As the potency of H_3R ligands decreases in calcium-free ACSF (CF-ACSF) when no endogenous histamine release occurs (De Luca et al. 2016), we tested whether OLHA inhibition is still present under this condition: significant excitation was observed in all 12 cells, when baseline was compared with activity during 19th to 25th min of experiment (Wilcoxon $p<0.05$) (Fig. 1A). The difference in occurrence of excitation vs inhibition and "no change" was significant between control (n=10) and CF-ACSF (n=12) FEPT p=0.0028. Comparison of control recordings in normal solution (NSOL) with the recordings in clobenpropit and in CF-ACSF using the Kruskal-Wallis test followed by Dunn´s multiple comparison test showed a difference ($H(2,N=29)=6.56$; $p=0.0375$). OLHA responses in CF-ACSF and in NSOL (Fig.1A, right plot) also were found to be different by the unpaired t-test ($t(20)=2.1$, $p=0.049$). Next, we compared kinetics of the RAMH ((*R*)-alpha-methyl-histamine, H_3R-agonist) and OLHA responses. We selected 4 cells inhibited by OLHA in NSOL (in one cell inhibition of firing by 0.27 Hz developed later but did not differ significantly from the baseline, Wilcoxon $p=0.18$). Responses to OLHA and RAMH differed in their time-course (2-way ANOVA-RM, difference in time factor $F(2,16)=7.13$, $p=0.0061$): while firing frequency was reduced during the application period of RAMH in all 6 cells (Fig.1C), the firing frequency was either increased or not changed during OLHA application (Fig.1C, right plot). Difference between data points was significant ($U(N1=6, N2=4) =0$; $p=0.0095$, MWT). The washout period was characterized by a similar reduction of firing frequency by both drugs with MWT $U=10$; $p=0.76$ (Fig. 1C). Thus, OLHA-induced inhibition of firing was delayed, likely through interaction with targets distinct from H_3R. Moreover, recordings in CF-ACSF revealed a clear-cut difference between RAMH and OLHA: while RAMH, as in NSOL, was inhibitory in CF-ACSF (frequency reduction by 1.23±0.03 Hz (n=5) during application period, difference from NSOL (n=6, see above) not significant, MWT $U(N1=6, N2=5)=10$; $p=0.43$), OLHA caused excitatory responses (Fig.1A,B). This excitation was dose-dependent and reached a maximum at the 21-

25th min of experiment with 0.25 ±0.17 Hz (n=22), 0.65 ±0.18 Hz (n=24) and 0.99±0.21 Hz (n=28) for concentrations of OLHA 10, 100 and 1000nM, respectively. At 5µM OLHA-induced responses were often transient with excitation followed by cessation of firing due to depolarization block or direct interaction with histamine 3 receptor. Therefore, in the majority of the following experiments OLHA was used at a concentration of 1µM.

3.3 OLHA-induced excitation of HA neurons is impaired by peroxisome proliferator-activated receptor-alpha (PPAR-alpha) antagonist and mimicked by the synthetic PPAR-alpha agonists.

Experiments performed in CF-ACSF showed that OLHA-induced excitation of HA neurons is sensitive to the PPAR-alpha antagonist MK886 (Fig. 2A) and is insensitive to the cannabinoid receptors antagonists AM251 and AM639 (Fig. 2B). As TRPV1 is a calcium- and sodium-permeable channel, we tested involvement of TRPV1 in the OLHA-action in normal solution with clobenpropit (20µM) to isolate the excitatory component of OLHA action. We found no difference in OLHA-excitation in control and in the presence of the TRPV1 antagonist AMG9810 (Fig. 2C). The partial and low efficacy PPAR-alpha activator gemfibrozil was inactive at concentration 1µM (Fig. 3A), whereas at 10µM it increased firing of TMN HA cells by 0.91±0.29Hz (n=14) in similar fashion to other PPAR-alpha activators taken at concentration 1µM: OLHA (1.02±0.24 Hz, n=26), OEA (1.15±0.32, n=10) and GW7647 (0.77±0.26, n=11). Note, that the highly potent and selective synthetic PPAR-alpha activator GW7647 (1µM) showed not only an action similar to OLHA but also shared the mechanisms of action (Fig. 3B,C). As a previous study has shown that translocation of PPAR-alpha after ligand binding from lipid droplets to the cell nucleus occurs in adipocytes within 5-15 minutes and depends on protein kinase A (PKA) activation (Mottillo et al. 2019), we tested whether an inhibitor of PKA can affect the response to PPAR-alpha activator in brain neurons: H-89 (10µM) significantly impaired responses to GW7647 (1µM) and to OLHA (1µM) (Fig. 3B,C). Neither the phospholipase C (PLC) blocker U73122 (5µM) nor the phosphatidylinositol-3-kinase (PI3K) inhibitor wortmannin (0.5µM) affected the OLHA response. Difference from OLHA -control (1µM, n=8 cells) at 15-22min of recording was calculated for experiments in U73122 with MWT (p=0.72, U(N1=8, N2=5)=17). Experiments in the presence of wortmannin (n=6) did not differ from OLHA control (n=7): unpaired t-test with Welch´s correction (t(5)=1.29, p=0.25). Increase in firing frequency by OLHA (1µM)

represented 0.74±0.49Hz (n=5) in U73122 and 0.85±0.33 Hz (n=6) in the presence of wortmannin.

3.4 Responses to OLHA in current clamp experiments

Whole-cell current clamp recordings were performed from HA neurons of TMNv, which were either identified by red fluorescence (Tmt-HDC mice) or by depolarizing action of clobenpropit 20µM. At 10nM OLHA significantly hyperpolarized 4 cells (Wilcoxon $p<0.05$, baseline vs 21st - 25th min of recording) and did not change membrane potential (MP) significantly in 3 cells (Fig. 4). Depolarization was prevailing in responses to 0.1µM or 1µM of OLHA (Fig.4A-C), an effect not affected by tetrodotoxin (TTX, 1µM) co-applied with 20µM gabazine ($GABA_AR$ antagonist) (U(N1=6, N2=5)=13; p=0.78). In both groups considered together OLHA 1µM significantly depolarized 8 cells, inhibited 2 cells and did not change MP in 1 cell. The occurrence of MP depolarization differed significantly between OLHA 10nM and 1µM: FEPT p=0.004. To test whether 10nM of OLHA can directly bind to H_3R we used the [^{3}H]-N$^\alpha$-methylhistamine displacement assay.

3.5 [^{3}H]-*N*$^\alpha$- methylhistamine hH_3R displacement assay

The affinities of histamine and OLHA have been determined by displacement assay at hH_3R with pKi values of 7.38 (C.I. (95%) 7.46, 7.31, n=5) and 6.51 (C.I. (95%) 6.67, 6.36, n=7), respectively. The Ki values from these experiments represented 42nM for histamine and 310nM for OLHA. The OLHA concentration-effect plot in Fig. 5A shows averaged data points of 7 experiments with 30nM of OLHA being the smallest concentration producing a significant effect; this concentration (shaded grey in Fig. 4A) will be further called “the threshold concentration”.

3.6 Histamine reuptake blocker blanks inhibition of firing frequency by OLHA 10nM

We have shown previously that the histamine reuptake blocker D-22 at 10nM affects kinetics of the histamine-evoked response in HA neurons of TMN recorded in cell-attached mode of voltage clamp (De Luca et al. 2016). D-22 applied now to HA neurons recorded in current clamp inhibited firing and hyperpolarized the membrane potential (Fig. 5B-D), an effect non-distinguishable in amplitude from the action of OLHA 10nM (Fig. 5C-D). In contrast, when

applied together with D-22, OLHA enhanced the firing, when compared to the D-22 alone (Fig. 5 B-C).

3.7 OLHA increases intracellular Ca^{2+} level in HA neurons

OLHA applied to the HDC-GCaMP6f mouse brain slices for 5minutes caused an increase in intracellular calcium level in 46.5% of histaminergic neurons of TMNv (40 out of 86 cells) to 16.4±2.1% of the maximum (Fig.6). The H_3R agonist RAMH caused a decrease in intracellular calcium (Fig. 6A). The occurrence of OLHA-induced calcium rise was significantly reduced in the presence of clobenpropit and the PPAR-alpha antagonist MK886 (4 cells out of 39, FEPT $p<0.0001$, Fig. 6B), but not in the presence of clobenpropit alone (17 cells out of 37, FEPT $p=1.0$). Application to the slices of the same CF-ACSF solution as used for the electrophysiology did not allow stable recordings, as calcium-dependent fluorescence disappeared soon after beginning the perfusion.

3.8 OLHA potency in CF-ACSF and expression of PPAR-alpha in TMN

We have shown previously that HA neurons of the mouse TMN express PPAR-alpha, TRPV1, GPR119 and CB2 and are likely negative for postsynaptic CB1 receptors (De Luca et al. 2018). As a difference between male and female mouse brains in the expression of PPAR-alpha was reported by Dotson et al. (2016), we investigated i) whether OLHA- responses show sex- or age- dependence; ii) whether mRNA levels encoding for PPAR-alpha differ in TMN regions of male vs female mice.

Two groups were built of adult and juvenile mice for each sex and responses to different concentrations of OLHA in CF-ACSF were compared (Supplementary Fig. 3). None of the concentrations tested elicited sex or age-dependent responses. When all recordings were considered OLHA increased firing of HA neurons with an EC_{50} 44nM (Fig. 7A).

Semiquantitative mRNA fold change analysis revealed that the TMN tissue from adult females did not show a difference from the adult male mice: 0.9±0.12 (P76.5±4.7, n=10) vs 1.0±0.1 (P77.2±3.3, n=11), respectively. Moreover, TMN of juvenile mice of different sexes presented significant difference neither from adult mice nor between them (one way ANOVA was applied for these 4 groups, $p=0.159$, $F(3,33)=1.84$). In juvenile mice PPAR-alpha

mRNA level was 1.85±0.7 (P11.6±0.4, 7 female mice) and 1.6±0.4 (P11.2±0.36, 9 males) (Fig.7B).

3.9 Computational results

Docking of either OEA or OLHA to PPAR-alpha rendered complex models with binding affinity values (-9.29 ± 0.06 and -9.45 ± 0.08 kcal/mol, respectively; see Table 1) comparable to that of their precursor OLA (-9.97 ± 0.06 kcal/mol). These values are higher than that of the partial agonist gemfibrozil (-9.03 ± 0.07 kcal/mol), but lower than that of the most potent synthetic agonist GW7647 (-12.10 ± 0.13 and -12.12 ± 0.11 kcal/mol for conformations A and B, respectively). The lower binding energies of OEA and OLHA with respect to GW7647 are not unexpected, considering that synthetic agonists exert their pharmacological effect by displacing the endogenous agonists (Kamata et al. 2020).

Fig. 8 shows the main interactions of the ethanolamine and histamine fragments of OEA and OLHA, respectively. Similar to the carboxylate group of OLA, the amide group of both OEA and OLHA form hydrogen bonds with Ser280, Tyr314, His440 and Tyr464 (see also Table 2). These four residues interact with most PPAR-alpha ligands (Kamata et al. 2020), including GW7647 and gemfibrozil (Supplementary Fig.6). Moreover, the described hydrogen bonds, in particular with Tyr464, are one of the requirements for the agonist activity of PPAR-alpha ligands, by helping stabilize the activated state of the so-called H12 or AF-2 helix (Moreno-Santos et al. 2014; Roy et al. 2016). Additionally, OLA, OEA and OLHA form hydrophobic interactions with Thr279, a residue located on helix H3. Kamata et al (2020) have shown that the most potent and efficient activators of PPAR-alpha (GW7647 and Pemafibrate, EC_{50} ~50nM) also interact with Thr279 (though via water-mediated hydrogen bonds), and thus stabilize helix H3 and the coactivator binding pocket.

However, compared to OLA, OEA and OLHA establish additional interactions with residues on helix H3 (Fig. 8 and Table 2). Since ligand interactions with helix H3 have been proposed to help maintain the H12 or AF-2 helix in the activated state (Zoete, Grosdidier, and Michielin 2007), this might explain why OEA and OLHA seem to activate the receptor (Takao et al. 2015 and this work, respectively), whereas OLA can bind but not activate PPAR-alpha (Kamata et al. 2020). In particular, both OEA and OLHA form a hydrogen bond with Gln277 (thanks to the polar groups of their ethanolamine and histamine fragments, respectively). Moreover, Phe273 can form a hydrophobic interaction with OEA or a pi stacking interaction with the histamine

aromatic ring of OLHA. GW7647 also interacts with Phe273 and Gln 277 (Kamata et al. 2020), thus underpinning the role of these H3 interactions in agonist activity. Altogether, our docking results further support the experimental evidence that OLHA acts as an activator of PPAR-alpha.

4 Discussion and conclusions

We demonstrate a dual action of OLHA on histaminergic neurons of the hypothalamus. Low nanomolar concentrations inhibited the firing frequency in the majority of investigated neurons through H_3R activation whereas micromolar concentrations excited HA neurons by interacting with PPAR-alpha. Inhibition was absent in presence of the H_3R antagonist clobenpropit and in nominally calcium-free ACSF (CF-ACSF). Previous studies indicated the absence of endogenous histamine release in CF-ACSF (Arrang, Garbarg, and Schwartz 1985; De Luca et al. 2016). Considering the maintenance of responses to the H_3R agonist in CF-ACSF (De Luca et al., 2016) we interpret our findings as indirect recruitment of H_3R: downstream to the increased endogenous histamine level due to the block of histamine uptake by OLHA. Experiments with the [^{3}H]-N^{α}-methylhistamine displacement assay at hH_3R indicated a potency (Ki) of OLHA (310nM) about 8 times lower than the potency of histamine (42nM) at hH_3R. This approach could however not provide an answer to the question whether OLHA acts as agonist or as an antagonist at H_3R. Further model systems must be employed to answer this question in the future. The determined OLHA threshold concentration (around 30nM) for interaction with hH_3R helped us to exclude this target in the OLHA 10nM action in brain slices. The histamine reuptake blocker D-22 blanked the inhibitory action of OLHA 10nM on neuronal firing. Considering all aforementioned arguments, we suggest an indirect activation of H_3R by OLHA 10nM through the increased release of endogenous histamine. In addition, besides HA cells, there are plenty of other cell types in mouse posterior hypothalamus (Mickelsen et al. 2020) and activation of excitatory H1R on dopaminergic neurons of TMN (De Luca et al, 2016) or on glial cells can also be expected after inhibition of histamine reuptake. OLHA effects on other cell types await investigation in the future.

Our further experiments on brain slices were performed with OLHA 1µM, as both components: inhibitory and excitatory- were clearly resolved at this concentration. Neither antagonists of cannabinoid receptors CB1 and CB2 (AM251 & AM630) nor of TRPV1

(AMG98001) changed the response to OLHA whereas the antagonist of PPAR-alpha MK886 (which blocks the action of oleoylethanolamide (OEA) in HA neurons (De Luca et al. 2018) impaired it. The classical synthetic PPAR-alpha agonists gemfibrozil and GW7647 acted similar to OLHA increasing the firing rate of HA neurons and, in accordance with previous studies, we confirmed the low potency of gemfibrozil (Kamata et al. 2020). The PKA inhibitor H-89 significantly impaired OLHA- and GW7647-excitation, showing that, as in adipocytes (Mottillo et al. 2019), PKA is an important regulator of PPAR-alpha trafficking and signaling in brain slices. Previous studies reported memory deficits in PPAR-alpha knockout mice accompanied by down-regulation of synaptic plasticity related genes in the hippocampus; they discovered dependence of PKA signal cascades on PPAR-alpha and vice versa (Roy et al. 2016; Roy and Pahan 2015). The excitatory action of OLHA 1µM in our study could be explained by membrane potential depolarization, an effect maintained under TTX and gabazine, indicating a direct postsynaptic action of OLHA on HA neurons. Sahlholm et al. (2012) showed that depolarization impairs the function of H_3R, therefore depolarization by OLHA (PPAR-alpha-dependent) may prevent hyperpolarization through H_3R at least in the beginning of the drug application period, explaining the biphasic response.

Intracellular imaging in HDC-GCaMP6f mice revealed a Ca^{2+} rise in response to OLHA 1µM and a decline in response to RAMH; the response to OLHA was reduced by MK886. Although previous studies have shown that male mice express higher levels of PPAR-alpha compared to females in peripheral tissues and in some brain regions (Dotson et al, 2016) we did not find a difference in expression of PPAR-alpha between female and male mice in TMN.

Estimation of OLHA EC_{50} yielded 44nM, which is comparable to the previously published data for OEA (120nM) (Astarita et al. 2006) or GW7647 (51.8 nM) (Kamata et al. 2020). GW7647 is considered to be the most efficient and most potent synthetic activator of PPAR-alpha used in many studies as positive control (Kamata et al. 2020; Ghosh et al. 2015).

Our study presents the neuromodulatory action of a by-product of histamine, which can spontaneously occur in histamine-producing cells and in body fluids where OLA is available. Concentration of OLA in human blood serum after 12 hrs fasting is about 130µM (Kamata et al. 2020). Similar features were ascribed recently to OLDA which is produced and metabolized in parallel to dopamine in catecholaminergic neurons (Sergeeva et al. 2017). This discovery has important consequences not only for better understanding the control of energy expenditure by histamine (Yasuda et al. 2004; Finlin et al. 2017) but also for the

better treatment of neurodegenerative diseases with pathological increase in OLA (Fanning et al. 2019). The wake-promoting H_3R antagonist/inverse agonist pitolisant tested now for the treatment of sleepiness in patients with neurodegenerative disorders (Schwartz and Lecomte 2016) may increase endogenous accumulation of OLHA which potentiates the action of histamine by decreasing its clearance (Courousse and Gautron 2015; Yoshikawa et al. 2013). Interestingly, impaired uptake of histamine by glial cells leads to its decreased degradation: Yoshikawa et al. (2013) showed that active HNMT is localized to the cytosol, suggesting that histamine transport into the cytosol is crucial for histamine inactivation. Thus accumulation of OLA and OLHA may change temporal and spatial dynamics of histaminergic transmission, however, how efficacy of the treatment by pitolisant may be affected under pathological conditions needs to be further analyzed, starting with mouse models of synucleinopathy (Fanning et al. 2019). Activation of PPAR-alpha by OLHA can be considered as neuroprotective by analogy with other previously studied compounds such as PEA (palmitoylethanolamide) (Agarwal, Yadav, and Chaturvedi 2017; Avagliano et al. 2016), gemfibrozil (Gottschalk et al. 2019) or OEA (Plaza-Zabala et al. 2010). Multiple processes are regulated by PPAR-alpha in the brain including energy homeostasis, mitochondrial fatty acids metabolism, oxidative stress and inflammation with the specific activators considered to be important for the improvement of brain function in neurodegenerative and neurodevelopmental disorders (Wojtowicz et al. 2020;Luo et al. 2020). Provensi and colleagues have shown, that the brain histaminergic system plays a permissive role in the anorectic action of OEA, one of the known PPAR-alpha activators (Provensi et al. 2014). The present study suggests that OLHA is an OEA-like endogenous biotransformation product of histamine. A previous study reported that OLHA has the strongest potency as PPAR-alpha agonist among a series of fatty acid amides tested in a liver cell line (Takao et al. 2015). To induce expression of PPAR-alpha targets, including Cpt1a, OLHA was used by Takao et al. (2015) at 20µM. It is worth noticing that in our study 0.01-1µM of OLHA was necessary to activate PPAR-alpha and increase neuronal excitability (estimated EC_{50} about 44 nM) whereas H_3R activation (during histamine reuptake block) dominated over excitation at OLHA 10nM. Further studies will be necessary to determine the endogenous level of OLHA under normal and pathological conditions. This will allow predictions regarding the therapeutic outcome of treatment with pitolisant in narcolepsy or Parkinson´s disease and

the role of the novel endogenous modulator OLHA for neuronal activity in the brain and for the central and peripheral control of energy expenditure by histamine.

Figure legends

Fig.1. OLHA-evoked inhibition of HA neurons depends on H_3R. (A) Left plot: Time course diagram of firing frequency change in control experiments performed in normal solution (NSOL) in control and in the permanent presence of the H_3R antagonist clobenpropit (clob, 20µM). middle plot: Time course diagram shows experiments in calcium-free ACSF (CF-ACSF). Right plot shows individual values from all experiments (averages of 19-25min of recording). Kruskal-Wallis test (p=0.0052) followed by Dunn´s multiple comparison test shows difference between OLHA effects in NSOL and CF-ACSF, but no difference between other pairs. (B) Example of extracellular action potential current (eAPC) recordings (in CF-ACSF) in one HA neuron; traces and averaged eAPC from these traces are shown. (C) Overlaid time course diagrams show difference in response kinetics in OLHA-inhibited cells when OLHA and the H_3R agonist R-alpha-methyl-histamine (RAMH, 2µM) are compared. Right plot shows individual values from these experiments which represent averages during the following time periods: 1) baseline, first 7 min of recording, 2) application period 7min, 3) 7min of post-application period or washout. Comparison of data points with MWT shows difference in responses during application phase (2) (U =0; p=0.0095) but not during phase (3) (U=10; p=0.76). For N1 and N2 (in MWT U) see number of cells (n) provided below time course diagrams.

Fig.2. OLHA-induced excitation of HA neurons is impaired by PPAR-alpha antagonist (A) Time course diagrams of averaged (±SEM) firing frequency changes in CF-ACSF experiments in control and in the presence of MK886 (1µM), individual values obtained during 19-25 min of experiment (averages) are shown in the right plot. Significance level (p) is determined by the unpaired t-test: t(20)=2.57. (B) Experiments in the permanent presence of CB1/CB2 antagonists AM251/ AM630 (each at 0.5µM) show no difference in OLHA action compared to the control experiments, individual values obtained during time period 19-25min were compared with the MWT: U=14. Number of recorded cells is shown below the time course diagrams. (C) Antagonist of TRPV1 (AMG9810, 3µM) does not change OLHA-induced excitation recorded in normal ACSF with clobenpropit (clob) 20µM. Comparison of individual values shown in right plot was done with MWT, U=13.

Fig.3. OLHA-induced excitation of HA neurons is mimicked by PPAR-alpha agonists. (A) Left plot shows individual responses (averages during the plot time period indicated above). Taken at 1µM gemfibrozil (gem) action on HA neurons is significantly different (no or slight increase in firing frequency, FFR) from OLHA (MWT, U=52) or OEA (unpaired t-test with Welch correction, t(11)=2,7). No difference between groups was detected with the Kruskal-Wallis test p=0.168. Right: representative traces of individual experiments show voltage clamp (Vh=0mV) cell attached firing rate recordings (B) The protein kinase A blocker H-89 (10µM) prevents excitation by OLHA. Individual values were compared with unpaired t-test, averages from 15 to 22min of experiment: t(8)=2.9, and from 23 to 29 min: t(8)=3.8. (C) The protein kinase A blocker H-89 (10µM) impairs excitation by GW7647 (difference between individual data points shown at the right side was calculated with unpaired t-test (t(16)=3.05 , upper plot) or with MWT (U=17, lower plot).

Fig.4. Membrane potential (MP) changes in response to different concentrations of OLHA.
(A) Averaged time course diagrams and (B) individual values for the periods 1 and 2 (labelled with open bars in (A)). Period 1(10-14min): one way ANOVA F(3,19)=1.6, p=0.22; Period 2 (21-25min): one way ANOVA F(3,19)=1.8, p=0.18. Significant difference after paired wise comparison was detected (see p values) between effects of OLHA 10nM and OLHA 1µM in TTX/gz (unpaired t-test t(10)=3.34) in (1) and between OLHA 10nM and OLHA 1µM in (2): t(11)=2.9. (C) Example of whole-cell current-clamp recording, where OLHA causes depolarization and increase in firing rate.

Fig.5. Response to OLHA 10nM is blanked by histamine reuptake blocker D-22.
(A) Specific binding of [^{3}H]-N^{α}-methylhistamine in the presence of increasing concentrations of OLHA. All data (dots represent averages of 7 independent experiments done in duplicates) are normalized on response to 0.3nM of OLHA (100%, or baseline), bars represent the means of normalized data. OLHA concentrations ≥ 30nM act significantly different from baseline as determined by 1-way RM ANOVA (F(6,6)=10.2, p<0.00001) with Dunnett´s multiple comparison test (exact p values are provided over the bars). (B) Time course diagrams of averaged firing frequency of HA neurons and their responses to D-22 alone or OLHA 10nM co-applied with D-22, results of current clamp experiments. Unpaired t-test shows difference (as indicated by p value) between two groups during period 15-22min (t(9)=2.65). (C) and (D) plots show individual values for the averaged time periods from experiments shown in (B) and control OLHA 10nM application shown in Fig. 4A. (C) Frequency change evaluated with one way ANOVA did not differ between 3 groups either during 10-14min period (left plot): F(2,14)=2.48, p=0.12, or during 15-22min period (right plot): F(2,14)=3.05, p=0.08. (D) one way ANOVA does not reveal difference in membrane potential change between groups: F(2,17)=0.126, p=0.88. Results shown in B-D were obtained from p13±0.7 mice (n=11).

Fig.6. OLHA increases intracellular calcium2+ level in HA neurons. (A) Left: Comparison of relative intracellular calcium levels in response to H_3R agonist RAMH and to OLHA, all responses normalized to the maximal fluorescence during kainate response (100%). Averages (±SEM) of 8 independent experiments are shown. Right: Photograph of one representative TMNv field and of the selected regions of interest (ROI: cell bodies) in this field, indicated with arrows. (B) comparison of data points within the washout period indicated by grey bar in (A) reveals significant difference between response to OLHA in the presence and absence of antagonists: clobenpropit 20µM (clob) and MK886 1µM (H(2,N=162)=29.8; p<0.0001), indicated pairs differ significant (***p<0.001), number of cells is given in brackets.

Fig. 7. Dose dependent OLHA-evoked excitation of HA neurons and semiquantitative analysis of PPAR-alpha expression in TMN. **(A)** Summary of all recordings performed in CF-ACSF in adult (ad) and juvenile (juv) mice of both sexes (fem: female, m: male). Time course diagrams of averaged (±SEM) firing frequency changes in response to OLHA. For individual data points see supplementary Fig. 3. Averages of 21st to 25th minute of recording period (marked by black line over the time scale in (A)) were used for the construction of dose-response curve shown in (B). Number of recorded cells is given in (A). (C) PPAR-alpha mRNA levels are not age-or sex-dependent in TMN. Dots represent averages of 2-4 amplifications, 1 dot per mouse.

Fig. 8. Comparison of the crystallographic pose of OLA with the docking poses of OEA and OLHA. The PPAR-alpha-OLA complex corresponds to PDB code 6LX8, whereas the best ranked docking poses according to the Haddock score are shown for OEA and OLHA. Receptor residues are shown as sticks with C atoms in cyan, whereas ligands are displayed as ball-and-sticks with C atoms in grey; N and O

atoms are colored in blue and red, respectively. Hydrogen bonds are indicated with black dashed lines and π stacking interactions with an orange arrow.

Supplementary Fig.1. OLHA 10nM- evoked responses in normal solution and in the presence of gabazine 10μM (GABAA receptor antagonist). (A) Examples of recorded slices (neurons of ventrolateral TMN were recorded either in whole coronal slice or in hemislice). Example of cell-attached voltage clamp recording of eAPCs is shown at right. (B,C) Averages of 3 time periods in individual experiments are connected by line. Difference from baseline was calculated with Wilcoxon signed rank test (exact p values are given for each individual cell): post-application period (15-21min) was compared with the baseline (each period contains 7 data points, one per minute), their averages are plotted vs time period in time-firing frequency change diagrams. Different symbols show recordings in different cells. Two different sets of neurons were recorded in (A) and (B). OLHA was applied only once to one neuron. One neuron per (hemi)slice was recorded.

Supplementary Fig.2. Examples of cell-attached voltage-clamp recordings of eAPCs (extracellular action potential currents) in control, during last minute of OLHA application and during 25th minute of experiment. Recordings were done in normal ACSF (NSOL: normal solution). Averaged eAPCs collected from traces above are shown at the bottom.

Supplementary Fig 3. Lack of age- or sex- dependence of OLHA excitation.

Individual data points (averages of 21st to 25th minutes of recording) show firing frequency change (FF Ch) for juvenile (juv) or adult (ad) female (F) or male (M) HA neurons in response to OLHA; concentrations are given at the left side. Results of ANOVA or Kruskal-Wallis (H) statistics are shown at the right side. Number of recorded neurons is given in brackets.

Supplementary Fig. 4. PPAR-alpha receptor structure used for molecular docking, based on PDB code 6LX8. The binding pocket for the polar head of OLA, OEA and OLHA is indicated with a dashed circle and the residues discussed in the text are shown as sticks (with C atoms in cyan, N in blue and O in red).

Supplementary Fig. 5. Chemical structures of the analyzed ligands: OEA (N-oleyl-ethanolamide), OLHA (N-oleoylhistamine), their precursor OLA (deprotonated oleic acid) and two synthetic PPAR-alpha agonists GW7647 and gemfibrozil.

Supplementary Fig. 6. (A)-(B) Crystal structure of PPAR-alpha in complex with GW7647 (PDB code 6KB3); two different ligand conformers were present, denoted A and B. (C) Docking pose of gemfibrozil in the Center/Arm I binding site (shown in Supplementary Figure 4). Binding of gemfibrozil to the secondary site in the Arm II/X region (Kamata et al. 2020) was not modeled in this work. In all three panels, receptor residues are shown as sticks with C atoms in cyan, whereas the ligand is displayed as ball-and-sticks with C atoms in grey; N and O atoms are colored in blue and red, respectively. Hydrogen bonds are indicated with black dashed lines.

Table 1. Binding affinities (ΔG_{bind}, in kcal/mol) calculated with PRODIGY-LIG for **(A)** all 200 PPAR-alpha complex models generated for each ligand and (B) only the top four models (ranked according to the Haddock score). The PPAR-alpha complex models correspond to dockings poses for OEA, OLHA and gemfibrozil and refined crystallographic poses for OLA and GW7647. Values in (A) correspond to mean± standard deviation.

(A)

Ligand	OLA	OEA	OLHA	GW7647 (conf. A)	GW7647 (conf. B)	Gem-fibrozil
ΔG_{bind}	-9.97 ±0.06	-9.29 ±0.06	-9.45 ±0.08	-12.10 ±0.13	-12.12 ±0.11	-9.03 ±0.07

(B)

Ligand	OLA				OEA				OLHA			
Pose	**#1**	**#2**	**#3**	**#4**	**#1**	**#2**	**#3**	**#4**	**#1**	**#2**	**#3**	**#4**
ΔG_{bind}	-10.0	-10.0	-10.0	-10.0	-9.4	-9.4	-9.3	-9.3	-9.5	-9.4	-9.5	-9.5

Ligand	GW7647 (conf. A)				GW7647 (conf. B)				Gemfibrozil			
Pose	**#1**	**#2**	**#3**	**#4**	**#1**	**#2**	**#3**	**#4**	**#1**	**#2**	**#3**	**#4**
ΔG_{bind}	-12.2	-12.3	-12.1	-11.8	-12.2	-12.1	-12.1	-12.1	-9.0	-9.1	-9.1	-9.0

Table 2. Protein-ligand interactions analyzed with PLIP for the top 4 ranked PPAR-alpha complex models of OEA and OLHA (docking poses), as well as the OLA (refined crystallographic poses). A filled box indicates the corresponding interaction is present, whereas a blank box denotes the interaction is absent.

Hydrogen bonds	**OLA**				**OEA**				**OLHA**			
Pose	**#1**	**#2**	**#3**	**#4**	**#1**	**#2**	**#3**	**#4**	**#1**	**#2**	**#3**	**#4**
Ser280												
Tyr314												
His440												
Tyr464												
Gln277												

π stacking interactions	**OLA**				**OEA**				**OLHA**			
Pose	**#1**	**#2**	**#3**	**#4**	**#1**	**#2**	**#3**	**#4**	**#1**	**#2**	**#3**	**#4**
Phe273												

Hydrophobic interactions	**OLA**				**OEA**				**OLHA**			
Pose	**#1**	**#2**	**#3**	**#4**	**#1**	**#2**	**#3**	**#4**	**#1**	**#2**	**#3**	**#4**
Ile241												
Ala250												
Glu251												
Leu254												
Val255												
Ile272												
Phe273												
Gln277												
Thr279												
Leu321												
Val332												
Ala333												
Ile354												
Val444												
Leu456												
Leu460												
Tyr464												

Table 2 (*cont.*). Protein-ligand interactions analyzed with PLIP for the top 4 ranked PPAR-alpha complex models of GW7647 (refined crystallographic poses) and gemfibrozil (docking poses). A filled box indicates the corresponding interaction is present, whereas a blank box denotes the interaction is absent.

Hydrogen bonds	**GW7647 (conf. A)**				**GW7647 (conf. B)**				**Gemfibrozil**			
Pose	**#1**	**#2**	**#3**	**#4**	**#1**	**#2**	**#3**	**#4**	**#1**	**#2**	**#3**	**#4**
Ser280												
Tyr314												
His440												
Tyr464												
Gln277												

Hydrophobic interactions	**GW7647 (conf. A)**				**GW7647 (conf. B)**				**Gemfibrozil**			
Pose	**#1**	**#2**	**#3**	**#4**	**#1**	**#2**	**#3**	**#4**	**#1**	**#2**	**#3**	**#4**
Phe218												
Ile241												
Leu247												
Leu254												
Val255												
Ile272												
Phe273												
Gln277												
Thr279*												
Thr283												
Tyr314												
Ile317												
Phe318												
Leu321												
Val332												
Ile354												
Val444												
Leu456												

* The water-mediated hydrogen bond between GW7647 and Thr279 (hydroxyl group) is not captured in our refined crystallographic poses because they do not contain water molecules. However, the distance between the NH (secondary amide) group of GW7647 (see Supplementary Figure 6A-B) and the hydroxyl group of Thr279 is still compatible with the presence of a water bridge (4.44 ± 0.28 Å and 5.32 ± 0.21 Å for the refined poses of conformations A and B, respectively, compared to 3.61 Å in the X-ray structure). Moreover, our analysis shows that the synthetic agonist can form an additional hydrophobic interaction with the methyl group of Thr279.

Acknowledgments

K.M. is associated member of interdisciplinary graduate school iBrain (Heinrich-Heine University, Düsseldorf). We are grateful to A. Scherer and K. Grau for excellent technical assistance as well as to I. Preljevic and M. Kocaoglu for synthesis support. Experiments on HEK293 cells were partially supported by the German Research Society (DFG INST 208/664-1 FUGG), GRK2158 and COST Actions CA15135, CA18133 and CA18240 to H.S.

Author Contributions

O.A.S., H.S., H.L.H. M.A.P. designed research, O.A.S., K.M, D.R.-L., K.L., M.A.P. performed research and analyzed data, O.A.S., H.L.H., K.M., M.A.P., H.S. wrote the paper. All authors worked on manuscript text and approved final version.

Additional information

All authors declare no competing financial interests.

Data availability

Data can be obtained upon request from the corresponding author

Reference List

Agarwal, S., A. Yadav, and R. K. Chaturvedi. 2017. 'Peroxisome proliferator-activated receptors (PPARs) as therapeutic target in neurodegenerative disorders', *Biochem.Biophys.Res.Commun.*, v.19;483: 1166-77.

Arrang, J. M., M. Garbarg, and J. C. Schwartz. 1985. 'Autoregulation of histamine release in brain by presynaptic H3-receptors', *Neuroscience*, 15: 553-62.

Astarita, G., B. Di Giacomo, S. Gaetani, F. Oveisi, T. R. Compton, S. Rivara, G. Tarzia, M. Mor, and D. Piomelli. 2006. 'Pharmacological characterization of hydrolysis-resistant analogs of oleoylethanolamide with potent anorexiant properties', *J Pharmacol Exp Ther*, 318: 563-70.

Avagliano, C., R. Russo, Caro C. De, C. Cristiano, Rana G. La, G. Piegari, O. Paciello, R. Citraro, E. Russo, Sarro G. De, R. Meli, Raso G. Mattace, and A. Calignano. 2016. 'Palmitoylethanolamide protects mice against 6-OHDA-induced neurotoxicity and endoplasmic reticulum stress: In vivo and in vitro evidence', *Pharmacol.Res.*, 113: 276-89.

Courousse, T., and S. Gautron. 2015. 'Role of organic cation transporters (OCTs) in the brain', *Pharmacol.Ther.*, 146:94-103. doi: 10.1016/j.pharmthera.2014.09.008.

De Luca, R., K. Mazur, A. Kernder, T. Suvorava, G. Kojda, H. L. Haas, and O. A. Sergeeva. 2018. 'Mechanisms of N-oleoyldopamine activation of central histaminergic neurons', *Neuropharmacology.*, 143:327-338. doi: 10.1016/j.neuropharm.2018.09.006.

De Luca, R., T. Suvorava, D. Yang, W. Baumgartel, G. Kojda, H. L. Haas, and O. A. Sergeeva. 2016. 'Identification of histaminergic neurons through histamine 3 receptor-

mediated autoinhibition', *Neuropharmacology.*, 106:102-15. doi: 10.1016/j.neuropharm.2015.08.025.

Dotson, A. L., J. Wang, Y. Chen, D. Manning, H. Nguyen, J. A. Saugstad, and H. Offner. 2016. 'Sex differences and the role of PPAR alpha in experimental stroke', *Metab Brain Dis.*, 31: 539-47.

Fanning, S., A. Haque, T. Imberdis, V. Baru, M. I. Barrasa, S. Nuber, D. Termine, N. Ramalingam, G. P. H. Ho, T. Noble, J. Sandoe, Y. Lou, D. Landgraf, Y. Freyzon, G. Newby, F. Soldner, E. Terry-Kantor, T. E. Kim, H. F. Hofbauer, M. Becuwe, R. Jaenisch, D. Pincus, C. B. Clish, T. C. Walther, R. V. Farese, Jr., S. Srinivasan, M. A. Welte, S. D. Kohlwein, U. Dettmer, S. Lindquist, and D. Selkoe. 2019. 'Lipidomic Analysis of alpha-Synuclein Neurotoxicity Identifies Stearoyl CoA Desaturase as a Target for Parkinson Treatment', *Mol.Cell.*, 73: 1001-14.

Finlin, B. S., B. Zhu, A. L. Confides, P. M. Westgate, B. D. Harfmann, E. E. Dupont-Versteegden, and P. A. Kern. 2017. 'Mast Cells Promote Seasonal White Adipose Beiging in Humans', *Diabetes*, 66: 1237-46.

Fleischer, W., S. Theiss, A. Schnitzler, and O. Sergeeva. 2017. 'Glutamine triggers long-lasting increase in striatal network activity in vitro', *Exp.Neurol.*, 290:41-52. doi: 10.1016/j.expneurol.2017.01.003.

Frick, M. H., O. Elo, K. Haapa, O. P. Heinonen, P. Heinsalmi, P. Helo, J. K. Huttunen, P. Kaitaniemi, P. Koskinen, V. Manninen, and et al. 1987. 'Helsinki Heart Study: primary-prevention trial with gemfibrozil in middle-aged men with dyslipidemia. Safety of treatment, changes in risk factors, and incidence of coronary heart disease', *N Engl J Med*, 317: 1237-45.

Ghosh, A., M. Jana, K. Modi, F. J. Gonzalez, K. B. Sims, E. Berry-Kravis, and K. Pahan. 2015. 'Activation of peroxisome proliferator-activated receptor α induces lysosomal biogenesis in brain cells: implications for lysosomal storage disorders', *J Biol Chem*, 290: 10309-24.

Gottschalk, C. G., A. Roy, M. Jana, M. Kundu, and K. Pahan. 2019. 'Activation of Peroxisome Proliferator-Activated Receptor-alpha Increases the Expression of Nuclear Receptor Related 1 Protein (Nurr1) in Dopaminergic Neurons', *Mol.Neurobiol.*, 56: 7872-87.

Haas, H. L., O. A. Sergeeva, and O. Selbach. 2008. 'Histamine in the nervous system', *Physiol Rev.*, 88: 1183-241.

Humphrey, W., A. Dalke, and K. Schulten. 1996. 'VMD: visual molecular dynamics', *J Mol Graph*, 14: 33-8, 27-8.

Kamata, S., T. Oyama, K. Saito, A. Honda, Y. Yamamoto, K. Suda, R. Ishikawa, T. Itoh, Y. Watanabe, T. Shibata, K. Uchida, M. Suematsu, and I. Ishii. 2020. 'PPARα Ligand-Binding Domain Structures with Endogenous Fatty Acids and Fibrates', *iScience*, 23: 101727.

Khanfar, M. A., D. Reiner, S. Hagenow, and H. Stark. 2018. 'Design, synthesis, and biological evaluation of novel oxadiazole- and thiazole-based histamine H(3)R ligands', *Bioorg.Med.Chem.*, 26: 4034-46.

Kim, C. K., S. J. Yang, N. Pichamoorthy, N. P. Young, I. Kauvar, J. H. Jennings, T. N. Lerner, A. Berndt, S. Y. Lee, C. Ramakrishnan, T. J. Davidson, M. Inoue, H. Bito, and K. Deisseroth. 2016. 'Simultaneous fast measurement of circuit dynamics at multiple sites across the mammalian brain', *Nat.Methods.*, 13: 325-28.

Koukos, P. I., L. C. Xue, and Amjj Bonvin. 2019. 'Protein-ligand pose and affinity prediction: Lessons from D3R Grand Challenge 3', *J Comput Aided Mol Des*, 33: 83-91.

Luo, R., L. Y. Su, G. Li, J. Yang, Q. Liu, L. X. Yang, D. F. Zhang, H. Zhou, M. Xu, Y. Fan, J. Li, and Y. G. Yao. 2020. 'Activation of PPARA-mediated autophagy reduces Alzheimer disease-like pathology and cognitive decline in a murine model', *Autophagy*, 16: 52-69.

Mickelsen, L. E., W. F. Flynn, K. Springer, L. Wilson, E. J. Beltrami, M. Bolisetty, P. Robson, and A. C. Jackson. 2020. 'Cellular taxonomy and spatial organization of the murine ventral posterior hypothalamus', *Elife*, 9.

Moreno-Santos, I., F. J. Pavón, M. Romero-Cuevas, A. Serrano, C. Cano, M. Suardíaz, J. Decara, J. Suarez, F. R. de Fonseca, and M. Macías-González. 2014. 'Computational and biological evaluation of N-octadecyl-N'-propylsulfamide, a selective PPARα agonist structurally related to N-acylethanolamines', *PLoS One*, 9: e92195.

Mottillo, E. P., H. Zhang, A. Yang, L. Zhou, and J. G. Granneman. 2019. 'Genetically-encoded sensors to detect fatty acid production and trafficking', *Mol Metab*, 29: 55-64.

Panula, P., P. L. Chazot, M. Cowart, R. Gutzmer, R. Leurs, W. L. Liu, H. Stark, R. L. Thurmond, and H. L. Haas. 2015. 'International Union of Basic and Clinical Pharmacology. XCVIII. Histamine Receptors', *Pharmacol.Rev.*, 67: 601-55.

Plaza-Zabala, A., F. Berrendero, J. Suarez, F. J. Bermudez-Silva, E. Fernandez-Espejo, A. Serrano, F. J. Pavon, L. H. Parsons, F. R. De Fonseca, R. Maldonado, and P. Robledo. 2010. 'Effects of the endogenous PPAR-alpha agonist, oleoylethanolamide on MDMA-induced cognitive deficits in mice', *Synapse*, 64: 379-89.

Provensi, G., R. Coccurello, H. Umehara, L. Munari, G. Giacovazzo, N. Galeotti, D. Nosi, S. Gaetani, A. Romano, A. Moles, P. Blandina, and M. B. Passani. 2014. 'Satiety factor oleoylethanolamide recruits the brain histaminergic system to inhibit food intake', *Proc.Natl.Acad.Sci.U.S.A*, 111: 11527-32.

Roy, A., M. Kundu, M. Jana, R. K. Mishra, Y. Yung, C. H. Luan, F. J. Gonzalez, and K. Pahan. 2016. 'Identification and characterization of PPARα ligands in the hippocampus', *Nat Chem Biol*, 12: 1075-83.

Roy, A., and K. Pahan. 2015. 'PPARα signaling in the hippocampus: crosstalk between fat and memory', *J Neuroimmune Pharmacol*, 10: 30-4.

Rubins, H. B., S. J. Robins, D. Collins, C. L. Fye, J. W. Anderson, M. B. Elam, F. H. Faas, E. Linares, E. J. Schaefer, G. Schectman, T. J. Wilt, and J. Wittes. 1999. 'Gemfibrozil for the secondary prevention of coronary heart disease in men with low levels of high-density lipoprotein cholesterol. Veterans Affairs High-Density Lipoprotein Cholesterol Intervention Trial Study Group', *N Engl J Med*, 341: 410-8.

Sahlholm, K., J. Nilsson, D. Marcellino, K. Fuxe, and P. Arhem. 2012. 'Voltage sensitivities and deactivation kinetics of histamine H3 and H4 receptors', *Biochim.Biophys.Acta.*, 1818: 3081-89.

Salentin, S., S. Schreiber, V. J. Haupt, M. F. Adasme, and M. Schroeder. 2015. 'PLIP: fully automated protein-ligand interaction profiler', *Nucleic Acids Res*, 43: W443-7.

Schwartz, J. C., and J. M. Lecomte. 2016. 'Clinical trials with H3-receptor inverse agonists: What they tell us about the role of histamine in the human brain', *Neuropharmacology*, 106: 35-36.

Sergeeva, O. A., A. N. Chepkova, N. Doreulee, K. S. Eriksson, W. Poelchen, I. Monnighoff, B. Heller-Stilb, U. Warskulat, D. HÇÏussinger, and H. L. Haas. 2003. 'Taurine-induced long-lasting enhancement of synaptic transmission in mice: role of transporters', *J.Physiol*, 550: 911-19.

Sergeeva, O. A., A. N. Chepkova, B. Gorg, Almeida F. Rodrigues, H. J. Bidmon, H. L. Haas, and D. Haussinger. 2020. 'Histamine-induced plasticity and gene expression in corticostriatal pathway under hyperammonemia', *CNS.Neurosci.Ther.*, 26: 355-66.

Sergeeva, O. A., L. R. De, K. Mazur, A. N. Chepkova, H. L. Haas, and A. Bauer. 2017. 'N-oleoyldopamine modulates activity of midbrain dopaminergic neurons through multiple mechanisms', *Neuropharmacology*, 119:111-122. doi: 10.1016/j.neuropharm.2017.04.011.

Takao, K., K. Noguchi, Y. Hashimoto, A. Shirahata, and Y. Sugita. 2015. 'Synthesis and evaluation of fatty acid amides on the N-oleoylethanolamide-like activation of peroxisome proliferator activated receptor alpha', *Chem.Pharm.Bull.(Tokyo).* 63: 278-85.

van Zundert, G. C. P., Jpglm Rodrigues, M. Trellet, C. Schmitz, P. L. Kastritis, E. Karaca, A. S. J. Melquiond, M. van Dijk, S. J. de Vries, and Amjj Bonvin. 2016. 'The HADDOCK2.2 Web Server: User-Friendly Integrative Modeling of Biomolecular Complexes', *J Mol Biol*, 428: 720-25.

Waterhouse, A., M. Bertoni, S. Bienert, G. Studer, G. Tauriello, R. Gumienny, F. T. Heer, T. A. P. de Beer, C. Rempfer, L. Bordoli, R. Lepore, and T. Schwede. 2018. 'SWISS-MODEL: homology modelling of protein structures and complexes', *Nucleic Acids Res*, 46: W296-W303.

Wojtowicz, S., A. K. Strosznajder, M. Jezyna, and J. B. Strosznajder. 2020. 'The Novel Role of PPAR Alpha in the Brain: Promising Target in Therapy of Alzheimer's Disease and Other Neurodegenerative Disorders', *Neurochem.Res.*, 45: 972-88.

Xue, L. C., J. P. Rodrigues, P. L. Kastritis, A. M. Bonvin, and A. Vangone. 2016. 'PRODIGY: a web server for predicting the binding affinity of protein-protein complexes', *Bioinformatics*, 32: 3676-78.

Yanovsky, Y., J. M. Zigman, A. Kernder, A. Bein, I. Sakata, S. Osborne-Lawrence, H. L. Haas, and O. A. Sergeeva. 2012. 'Proton- and ammonium-sensing by histaminergic neurons controlling wakefulness', *Front Syst.Neurosci.*, 6:23. doi: 10.3389/fnsys.2012.00023.

Yao, B. B., C. W. Hutchins, T. L. Carr, S. Cassar, J. N. Masters, Y. L. Bennani, T. A. Esbenshade, and A. A. Hancock. 2003. 'Molecular modeling and pharmacological analysis of species-related histamine H(3) receptor heterogeneity', *Neuropharmacology*, 44: 773-86.

Yasuda, T., T. Masaki, T. Sakata, and H. Yoshimatsu. 2004. 'Hypothalamic neuronal histamine regulates sympathetic nerve activity and expression of uncoupling protein 1 mRNA in brown adipose tissue in rats', *Neuroscience*, 125: 535-40.

Yoshikawa, T., F. Naganuma, T. Iida, T. Nakamura, R. Harada, A. S. Mohsen, A. Kasajima, H. Sasano, and K. Yanai. 2013. 'Molecular mechanism of histamine clearance by primary human astrocytes', *Glia.*, 61: 905-16.

Zoete, V., A. Grosdidier, and O. Michielin. 2007. 'Peroxisome proliferator-activated receptor structures: ligand specificity, molecular switch and interactions with regulators', *Biochim Biophys Acta*, 1771: 915-25.

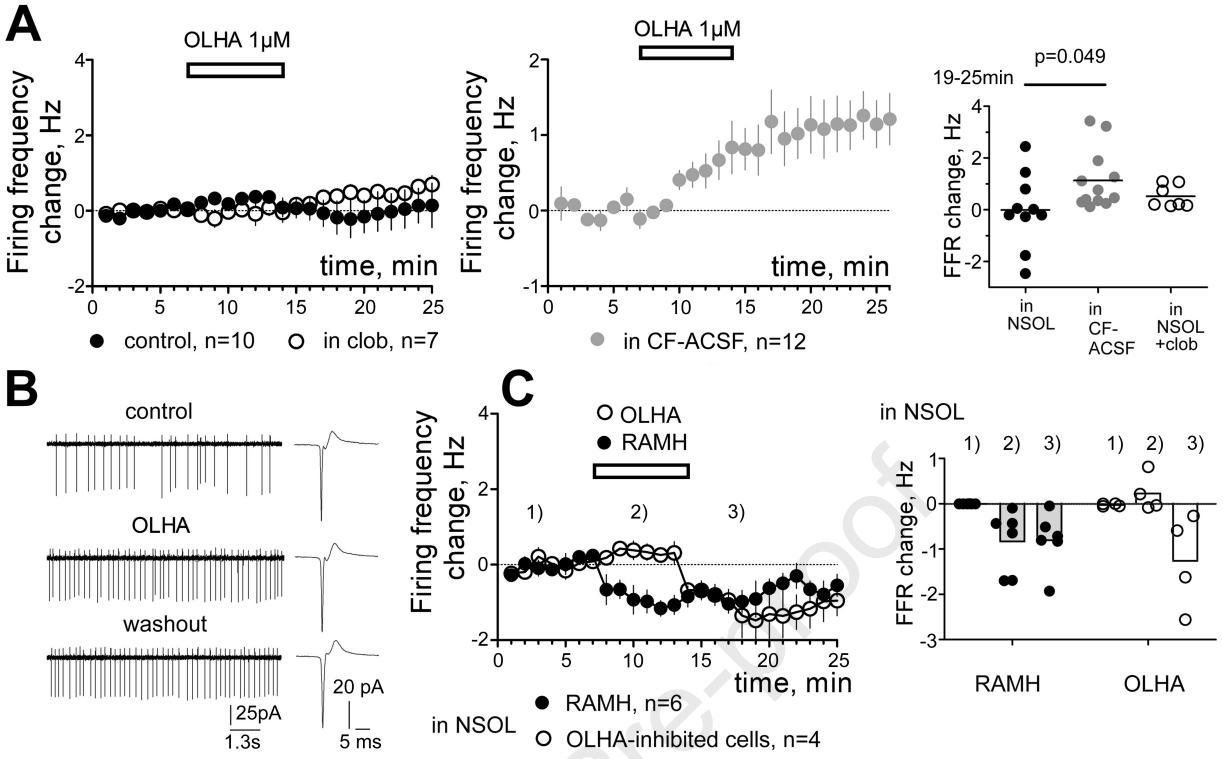

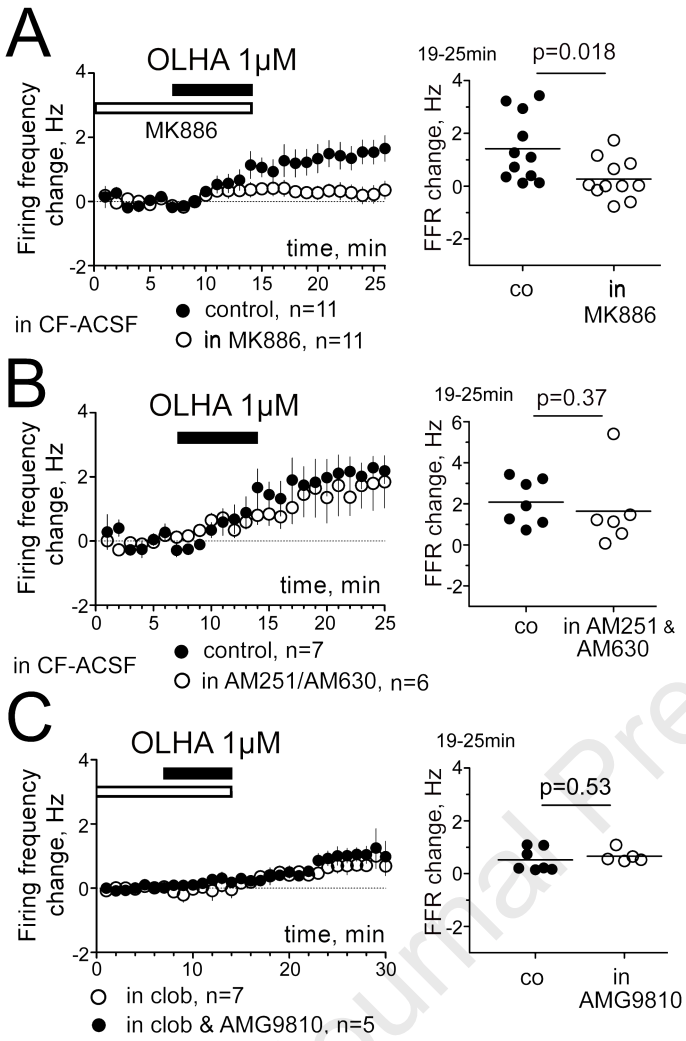

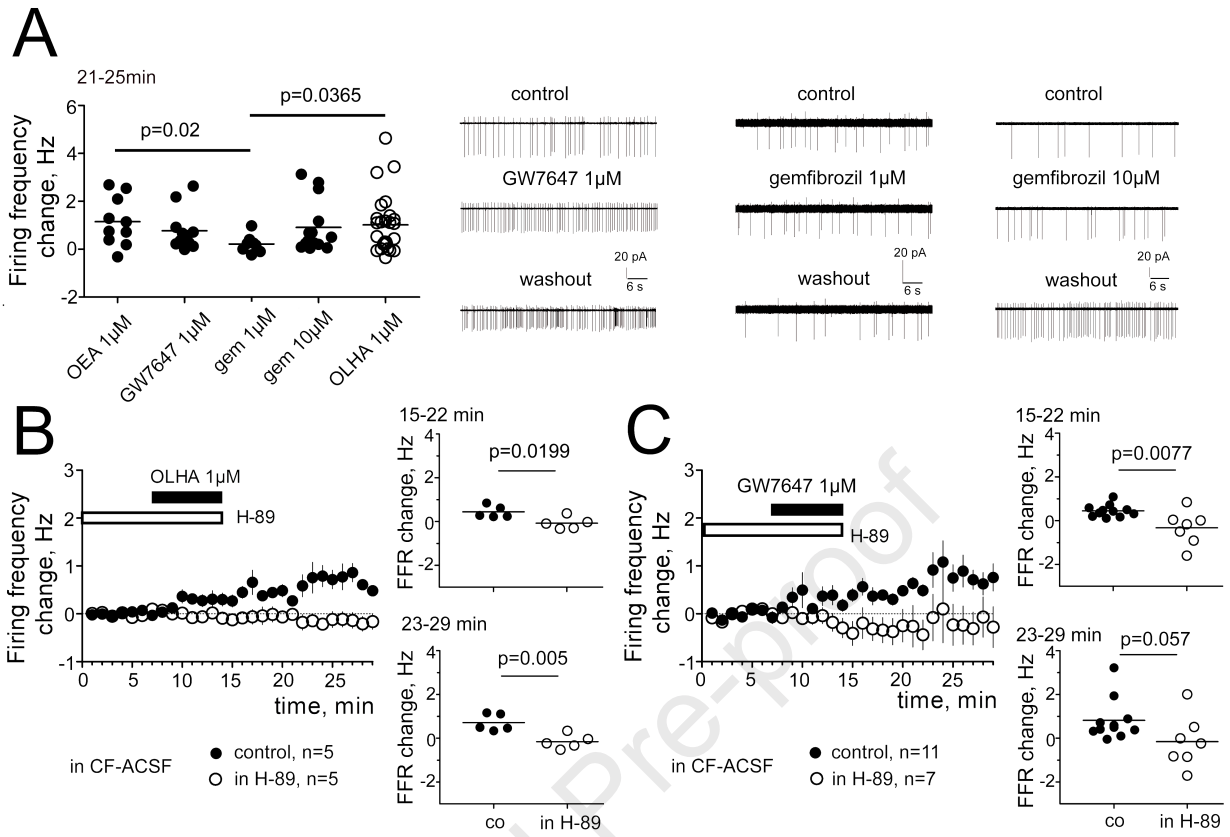

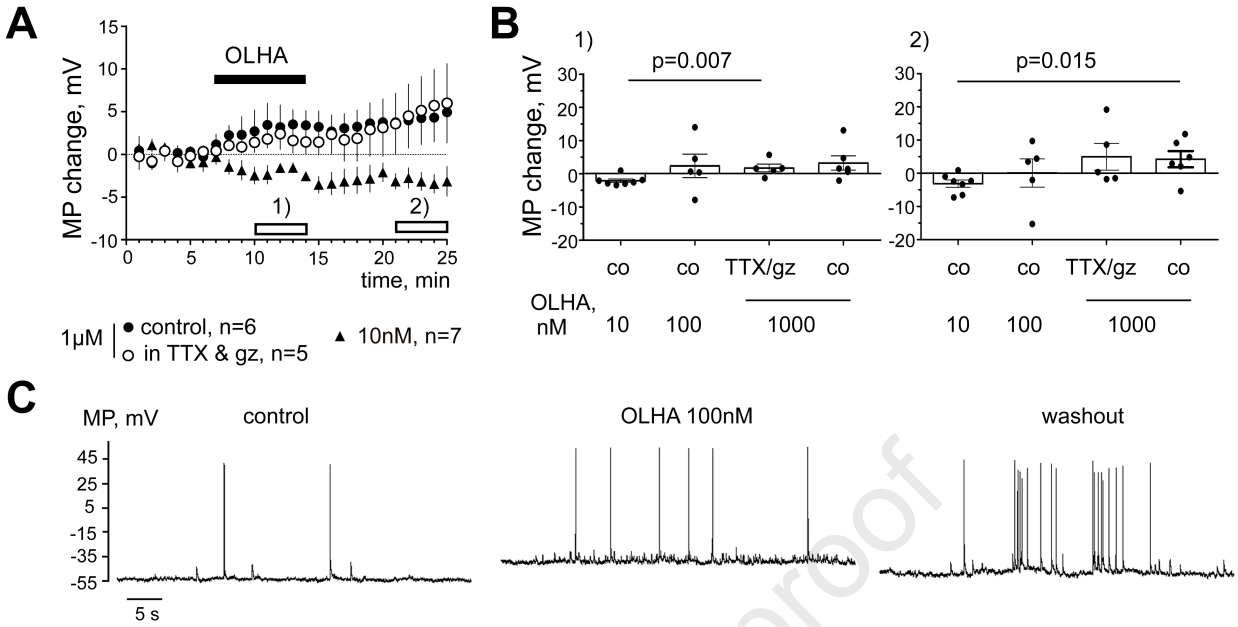

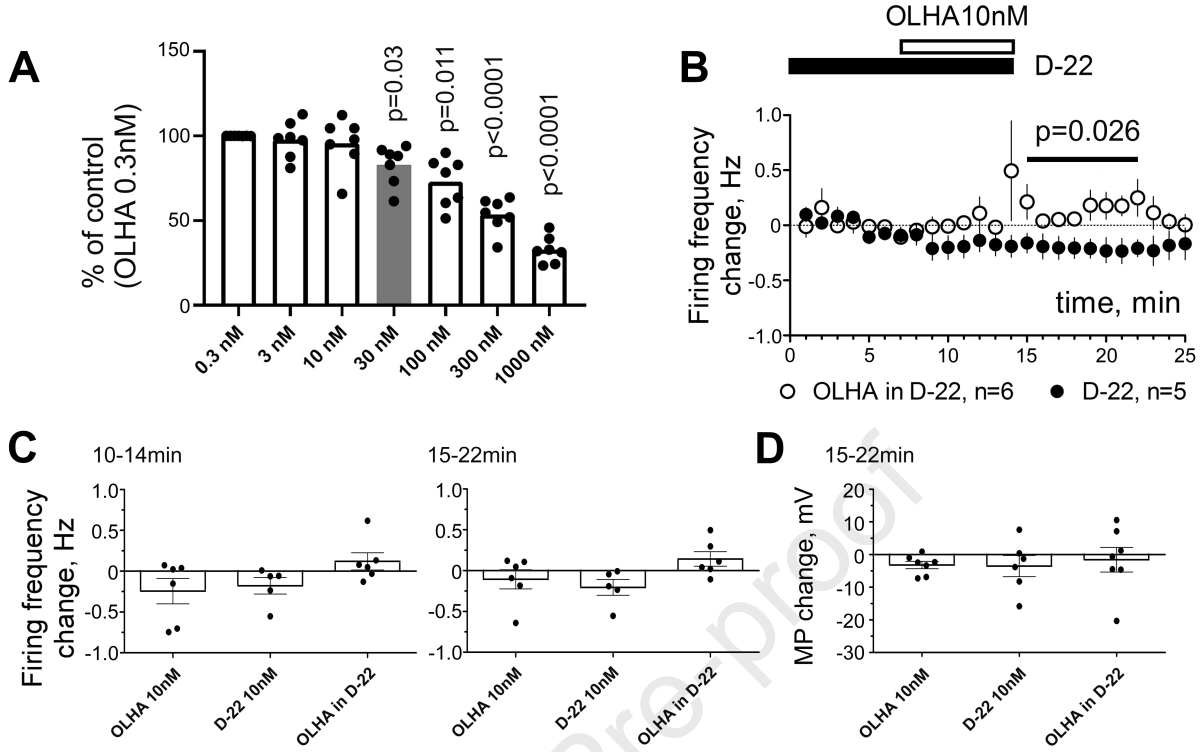

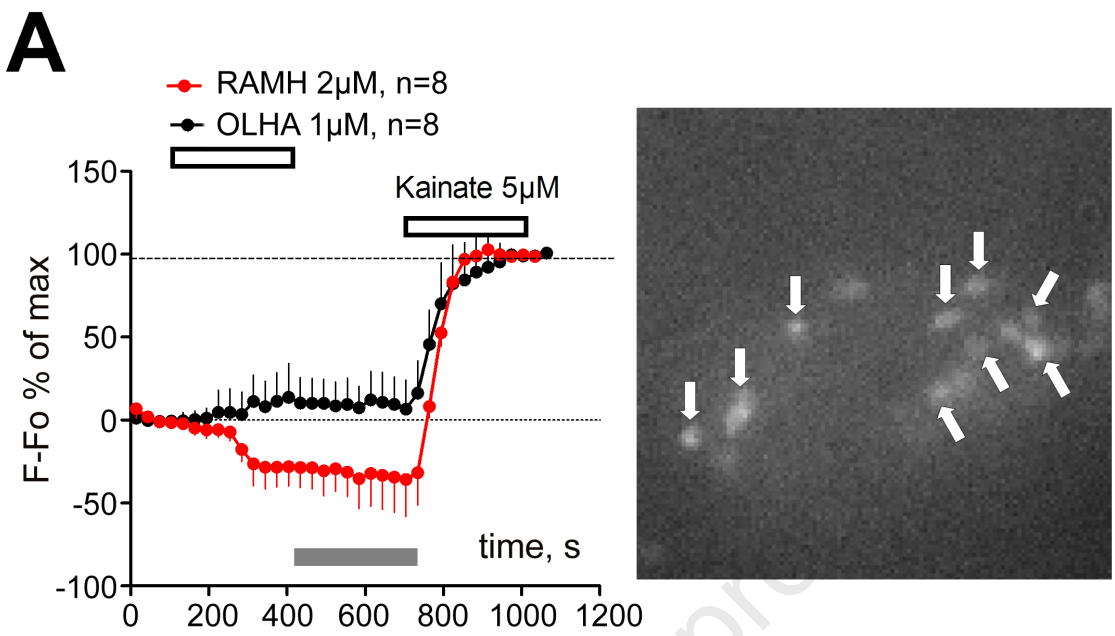

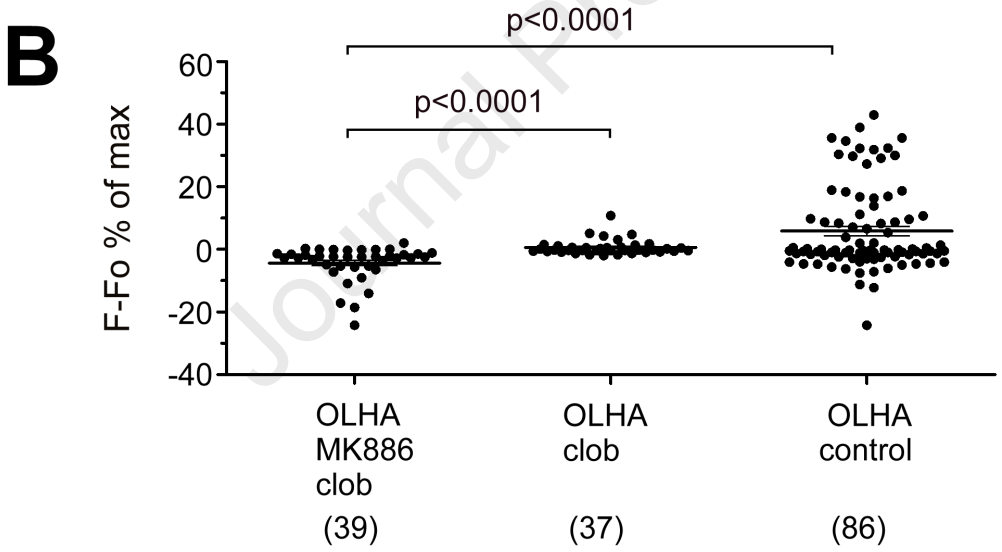

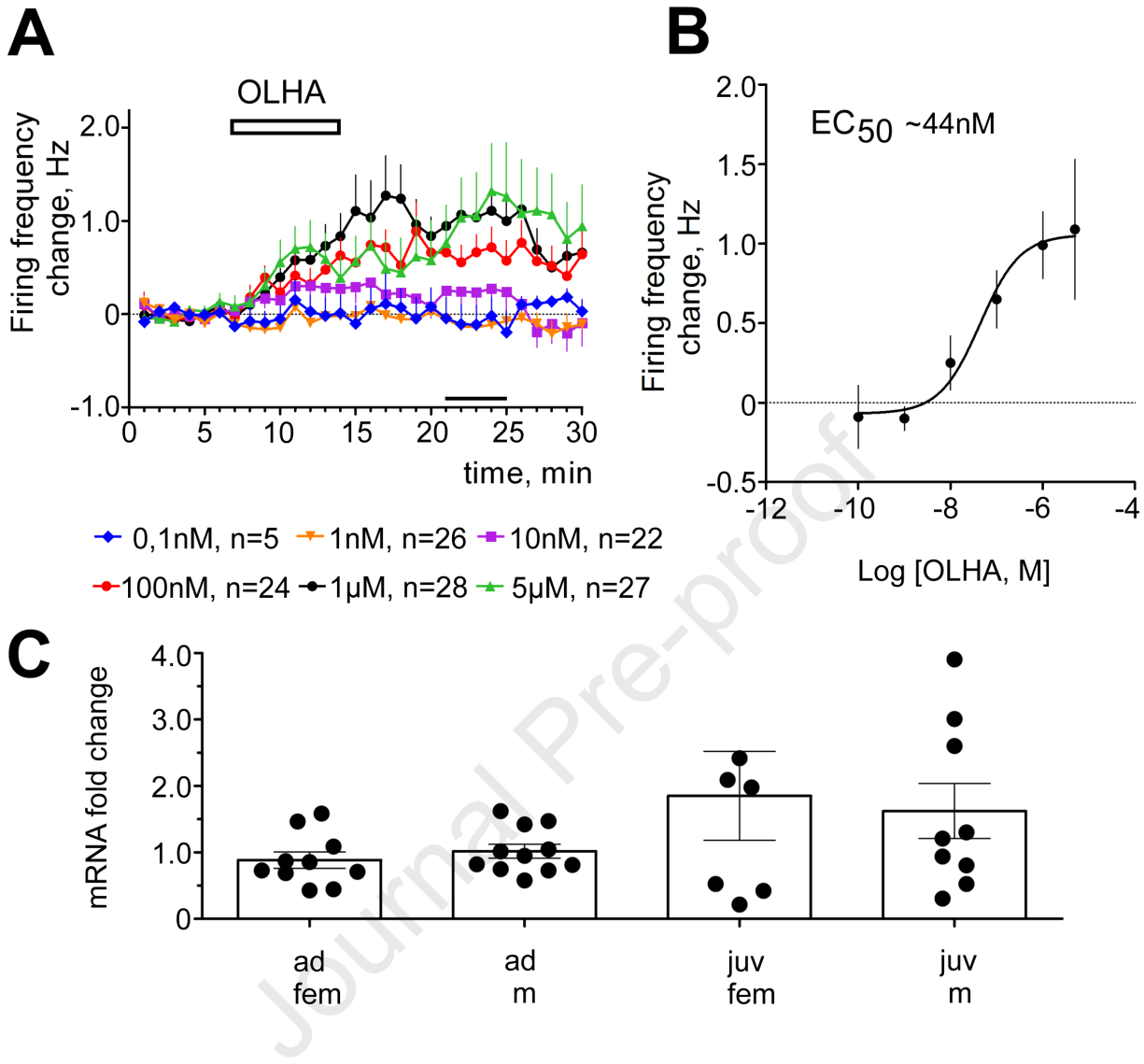

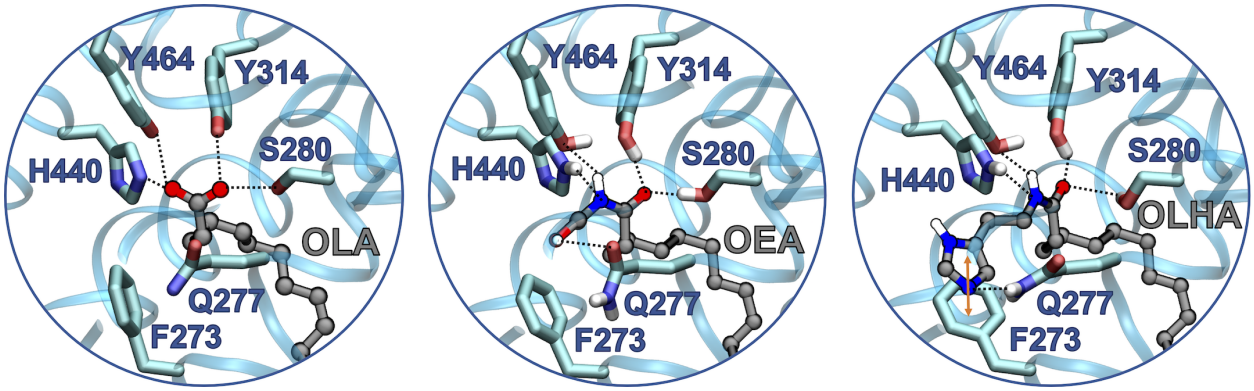

OLHA bidirectionally modulates histaminergic neuron firing.

Histamine 3 receptor and PPAR-alpha are involved in inhibition and excitation respectively.

OLHA interacts with histamine reuptake and may modulate histaminergic transmission under pathological conditions